

Technical potential assessment of offshore wind energy over shallow continent shelf along China coast



Bingchuan Nie ^{a, b, **}, Jiachun Li ^{c, d, *}

^a School of Civil Engineering, Beijing Jiaotong University, Beijing 100044, China

^b Beijing's Key Laboratory of Structural Wind Engineering and Urban Wind Environment, Beijing 100044, China

^c Key Laboratory for Mechanics in Fluid Solid Coupling System, Institute of Mechanics, Chinese Academy of Sciences, No.15 Beisihuanxi Road, Beijing 100190, China

^d School of Engineering Science, University of Chinese Academy of Science, Beijing 100049, China

ARTICLE INFO

Article history:

Received 13 November 2017

Received in revised form

2 May 2018

Accepted 23 May 2018

Available online 28 May 2018

Keywords:

Wind energy

Offshore wind farm

Floating wind turbine

GIS

Surface roughness length

ABSTRACT

Offshore wind resource assessment seems to be urgently needed due to the rapid development of offshore wind energy in the coming decades. Technical potential of offshore wind energy over the sea area shallower than 250 m along China coast is investigated. To avoid erroneous estimation of wind power density, a statistical model considering sea state effect is proposed. Long-term CCMP wind field data are examined using that model to reduce uncertainties. Further, influential factors including wind power density, water depth, wind turbine size, wind farm layout and various spatial constraints are analyzed on the GIS platform. Technical potential under different scenarios are presented and discussed. It shows that wind resource at Taiwan Strait is particularly abundant, where wind power density at 70 m height can be above 900 W/m². Technical potential is quite sensitive to the size of wind turbine. Taking the layout S1 (8 × 15 turbines in each farm, 8 rotor diameters apart between wind turbines, 20 km buffer region between neighboring farms) as an example: the total technical potential of the study area is 613 GW for rotor radius 60 m, and that for rotor radius 90 m is 1264 GW; the growth rates of technical potential with rotor radius is 19.3 GW/m roughly. Spatial constraints has significant impact on the region with water depth less than 50 m, where only 48.1% of area is available for developing wind energy and the technical potential there is about 23% of that of the study area.

© 2018 Elsevier Ltd. All rights reserved.

1. Introduction

Offshore wind energy experienced a recordable period and exhibits great growth potential in the coming years because of its advantages in larger wind speed, lower wind shear, fewer noise constraints and less land occupation. By the end of 2017, the global cumulative capacity reached 18.81 GW, in which 15.73 GW was newly installed during 2011–2017 according to Global Wind Energy Council (GWEC) [1]. The new intermediate scenario by European Wind Energy Association (EWEA) claimed that 66 GW offshore capacity is expected to be added in EU by 2030, and those

of the high/low scenario is 45 GW/98 GW [2]. National Renewable Energy Laboratory (NREL) predicted 38 GW of installed capacity is expected to be commissioned by 2020 in US, which would bring the cumulative installed capacity to 47 GW [3]. Recently, a plan “The Electric Power Development Planning in 13th Five-Year (2016–2020)” was released by the National Energy Administration of China (CNEA), which sets a goal of offshore wind capacity by 2020: 5 GW under commercial operation and 10 GW under construction [4].

Offshore wind resource assessment plays an important role in developing offshore wind energy. It can be usually classified into two scales, i.e. wind farm and regional scales. As for the wind farm scale, the accuracy of prediction of the annual energy production is the overriding concern, which is fluctuated by various uncertainties such as wind measurement, thermal stability of marine boundary layer and climate change. While the regional scale wind resource assessment is aimed to obtain the technical wind energy potential which will be helpful for the future offshore wind energy planning

* Corresponding author. Key Laboratory for Mechanics in Fluid Solid Coupling System, Institute of Mechanics, Chinese Academy of Sciences, No.15 Beisihuanxi Road, Beijing 100190, China.

** Corresponding author. School of Civil Engineering, Beijing Jiaotong University, Beijing 100044, China.

E-mail addresses: bcnie@bjtu.edu.cn (B. Nie), jcli05@imech.ac.cn (J. Li).

and the development of the offshore wind turbines. In this work, the regional scale wind energy potential over the sea area shallower than 250 m along China coast are investigated.

China's pilot offshore wind farm right nearby the Donghai Bridge was built in 2005 and the cumulative offshore wind capacity has hit 2.79 GW by the end of 2017. Wind energy potential over the coastal and tidal regions of Bohai Sea, Yellow Sea and East China Sea were firstly investigated by China Meteorological Administration (CMA) using the numerical model WERAS/CMA [5]. With the aid of MM5 model, Qin et al. [6] evaluated the offshore wind energy along the China coast at 100 m hub height. Hong et al. [7] investigated available offshore wind energy over the exclusive economic zone (EEZ) of China considering technical, spatial and economic constraints. Li et al. [8] investigated the climatology, variability, and extreme climate of winds over Bohai Sea and Yellow Sea using a regional climate model COSMO-CLM. And they also reviewed the other works related to wind resource over the seas of China before 2016, e.g. Refs. [9–11]. The geographical distribution of wind power density (WPD) over the seas of China has been uncovered preliminary owing to those works. However, the offshore wind energy potential over the seas of China are not complete yet. The major limitations of the previous works are: 1) most of the wind energy potential are at a few low heights which seems to be incompetent for the large-size modern wind turbines; 2) theoretical wind energy potential over China Seas such as 883 GW [12] (water depth 0–50 m, height 10 m), 660 GW [13] (region 10 km offshore, height 10 m) and 2000 GW [5] (water depth 5–25 m, height 50 m) are seldom available even seem to be contradictory; 3) technical wind energy potential have been discussed scarcely.

Three kinds of wind speed data are often used for wind resource assessment. One is from the in-situ measurement platforms such as meteorological masts, weather stations, ships and buoys. However, offshore observation platforms are quite rare due to the high costs of installation and maintenance. Additionally, the in-situ measured wind speed data are always point measurement with low spatial coverage limiting their application in regional scale wind resource assessment. Wind field data from numerical models with high temporal and spatial resolutions have also been using for offshore wind resource assessment. Ulazia et al. [14] estimated the wind energy potential in the Bay of Biscay relied on the mesoscale model WRF with/without 3DVAR data assimilation. They concluded that wind data obtained with data assimilation has better accuracy than that without data assimilation. Mattar [15] estimated the offshore wind energy potential for the central coast of Chile by WRF and wind speed data from in-situ stations and ERA-Interim reanalysis. Amirinia et al. [16] evaluated the wind and wave energy potential over Caspian Sea using the ECMWF wind data in which the QuikSCAT data are assimilated. Other numerical models such as MM5 [17,18], PROTHEUS [19] and COSMO-CLM [8] have also been relied on for offshore wind resource assessment. Ocean surface responds to wind forcing on many wavelengths providing a mechanism for the microwave remote sensing of ocean surface wind from space, which is competent to offshore wind resource assessment as well. Capps et al. [20] evaluated global offshore wind energy potential using 7 years QuikSCAT wind speed data. Hasager et al. [21] mapped the wind resource over Baltic Sea using the data from Advanced SAR on-board Envisat satellite. Gadad et al. [22] investigated the offshore WPD at 10 m and 90 m over Karnataka state in India using Oceansat-2 scatterometer wind data. Those satellite based wind field data have high spatial coverage. And their quality can be highly improved with the help of the aforementioned traditional in-situ measured wind data [23,24]. Since the regional scale wind resource assessment has lower requirement of temporal and spatial resolutions than that of the wind farm scale, it seems that using satellite based wind field data directly rather than

numerical products may gain a more accurate estimation of regional offshore wind resource. Because the analysis and reanalysis datasets based on satellite observations are often used as inputs for the numerical models, which means deviations of numerical products come from the numerical model itself and the observations.

As we know, the satellite based wind field data are often adjusted to a common reference height, say 10 m. To obtain an adequate estimation of WPD at hub height of modern wind turbines, say 90 m for 5 MW [25] even 120 m for 10 MW [26], precise vertical extrapolation of wind speed is a key problem to be solved. The logarithmic law and power law are the most commonly used wind profile during extrapolation. As for the logarithmic law wind profile, a constant sea surface length is usually assumed for the study area in literature, say 0.2 mm, e.g. Refs. [7,12,13,22]. In the power law wind profile model, the power index has also been regarded as a constant neglecting the influence of sea state, e.g. Refs. [27,28]. However, sea surface roughness length can vary in several decades due to the evolution of wave height and shape [29]. Inaccurate estimation of sea surface roughness will certainly introduce deviation of wind speed at hub height. Even worse, the deviation will be further enlarged in WPD, which is proportional to cube of wind speed. To estimate the sea surface roughness length considering sea state effect, recently, Amirinia et al. [16,30] used the wave parameters simulated by wave model SWAN. Since the marine boundary layer has been extensively studied with a lot of achievements available, developing a statistical model filling the gap between the present understanding of marine boundary layer and the requirement of regional scale offshore wind resource assessment may be another way out. However, in the authors' knowledge, such a statistical technical wind energy potential model is still blank yet.

In this work, a statistical model considering sea state effect is proposed and discussed for calculating technical potential in Section 2; based on that, influential factors related to developing offshore wind energy such as wind power density, water depth, wind farm layout and various spatial constraints are examined on the GIS platform; regional scale technical potential of offshore wind energy over the sea area shallower than 250 m along China coast under different scenarios are presented in Section 4; finally, Section 5 brings this study to a few conclusions.

2. Technical potential model considering sea state effect

2.1. WPD at reference height

The available wind energy potential per unit area perpendicular to the air flow, i.e. WPD, is expressed as

$$P = \frac{1}{2} \rho v^3, \quad (1)$$

where ρ and v are air density and wind speed, respectively. P is usually regarded as a scalar though v is a three dimensional vector, since the wheel of horizontal axis wind turbines can always be adjusted to oriented perpendicular to wind direction.

The random single-site wind speed series at reference height v_0 can be regarded as

$$v_0 = \bar{V} + \Delta V. \quad (2)$$

Where, mean wind speed \bar{V} is almost stable in the lifecycle of wind turbines; deviation ΔV can be treated as a random series reflecting the influences of short-term weather pattern and turbulent fluctuation. Then, the corresponding mean WPD at

reference height can be estimated by Eq. (3).

$$E_0 = \frac{1}{2}\rho_0\bar{V}^3 + \frac{3}{2}\rho_0\bar{V}E(\Delta V^2) + \frac{1}{2}\rho_0E(\Delta V^3). \quad (3)$$

Where $E(\cdot)$ denotes mathematical expectation, ρ_0 is air density at reference height. The geographical distribution of WPD at reference height can be obtained via Eq. (3) when the appropriate wind field data are given. Areas with relatively high wind energy potential can be singled out for optimal site selection of wind farms. However, hub height of large multi-MW wind turbine can be as high as, say 90 m for 5 MW, WPD at hub height need to be examined.

2.2. WPD at hub height considering sea state effect

Marine atmospheric boundary has profound impact on wind

$$\phi(\Delta V, \bar{V}) = \frac{\ln(f_*(\bar{V} + \Delta V)) - \ln(f_*(\bar{V}))}{[\ln(10) - \ln(z_0 f_*(\bar{V} + \Delta V)/g)] [\ln(10) - \ln(z_0 f_*(\bar{V})/g)]}. \quad (10)$$

speed profile mainly by its thermal stratification state and underlying surface, i.e. sea state. Diurnal cycles of SST and atmospheric stability are nearly absent due to the large heat capacity of sea water [29]. The Obukhov length scale is usually used as the stability parameter of the atmospheric boundary layer. The stability of the atmospheric boundary layer can be classified into very stable, stable, near neutral/stable, neutral, near neutral/unstable, unstable and very unstable. Most of the time, the marine atmospheric boundary layer is neutral or near neutral stratified [31]. As a result, wind speed at height z can be extrapolated from v_0 using the logarithmic wind profile under the neutral stratification assumption as

$$\frac{v(z)}{v_0} = \frac{\ln(z) - \ln(z_0)}{\ln(10) - \ln(z_0)}. \quad (4)$$

The well-known Charnock formula suggests that sea surface roughness length z_0 can be expressed as

$$z_0 = z_{0*} u_*^2 / g. \quad (5)$$

where g the gravity acceleration and u_* the friction velocity. z_{0*} , the so-called Charnock parameter, equals to 0.011 for open seas [32].

Friction velocity u_* is dependent on the wind speed v_0 and drag coefficient C_D . In the previous decades, both experimental and numerical observations have been carried out for the drag coefficient C_D (see the review [33]). For example, Li et al. [34] obtained the two-parameter-dependent drag coefficient relation based on Maat's work of regression analysis of HEXMAX data [35]. It confirmed that C_D increases with wind speed with slight variations due to wave age. That is to say, sea surface roughness length mainly related to the wind speed and wave age, which can be generally written as

$$z_0 = \frac{z_{0*}}{g} \cdot \text{Func.}(c_p/u_*, v_0). \quad (6)$$

However, it is still hard to obtain the real-time distribution of wave age over regional scale sea surface by now. A practical way is to seek the statistical relation between u_*^2 and v_0 as written by Eq. (7) based on the in-situ observation, in which wave age effect is considered statistically.

$$u_*^2 = f_*(v_0). \quad (7)$$

Then, the wind speed adjustment factor in Eq. (4) can be decomposed as

$$\frac{v(z)}{v_0} = 1 + \xi(z, \bar{V}) + \ln(z/10)\phi(\Delta V, \bar{V}). \quad (8)$$

Where $\xi(z, \bar{V})$ expressed as Eq. (9) reflects the influence of long-term mean wind speed; $\phi(\Delta V, \bar{V})$ reflects the impact of short-term wind speed deviation as shown in Eq. (10).

$$\xi(z, \bar{V}) = \frac{\ln(z) - \ln(10)}{\ln(10) - \ln(z_0 f_*(\bar{V})/g)}. \quad (9)$$

To determining $\xi(z, \bar{V})$ and $\phi(\Delta V, \bar{V})$, we shall found out the expression of u_*^2 i.e. Eq. (7), which turns into figuring out the statistical relation between drag coefficient C_D and v_0 . Relied on the experimental results by Smith [32], Large and Pond [36], Yelland and Moat et al. [37] and Foreman and Emeis [38], $f_*(v_0)$ can be obtained as listed in Table 1.

From Table 1, we can say u_*^2 have the same form as Eq. (11) with the unknown coefficients A, B, C, D and E . And those coefficient are evaluated by polynomial fitting as indicated by the solid line in Fig. 1 quantitatively: $A = -4.347 \times 10^{-6}$, $B = 2.732 \times 10^{-4}$, $C = -2.760 \times 10^{-3}$, $D = 2.042 \times 10^{-2}$, $E = -0.03576$. Consequently, $\xi(z, \bar{V})$ can be figured out using Eqs. (9) and (11).

$$f_*(v_0) = Av_0^4 + Bv_0^3 + Cv_0^2 + Dv_0 + E. \quad (11)$$

$\phi(\Delta V, \bar{V})$ in Eq. (10) is further depicted as shown in Fig. 2 using Eq. (11) to seek a reasonable simplification. It shows that $\phi(\Delta V, \bar{V})$ is in fact insensitive to \bar{V} for the common long-term mean offshore wind speed 5–8 m/s. Moreover, it is straightforward that $\phi(0, \bar{V})$ equals to zero according to Eq. (10). Thus it is reasonable to approximately evaluate $\phi(\Delta V, \bar{V})$ by a linear function of ΔV as

$$\phi(\Delta V, \bar{V}) = \kappa \Delta V. \quad (12)$$

Where constant coefficient κ is taken as $0.0019 \text{ (m/s)}^{-1}$ in this work as suggested by the linear fitting, that is the solid line in Fig. 2. From Fig. 2, the bias of ϕ due to simplification is less than 0.005 in general. According to Eq. (8), the simplification of ϕ can introduce deviation 1% maximal for wind speed for wind turbine hub height,

Table 1
Results on relationship between friction velocity and wind speed.

Ref.	u_*^2	Effective range (m/s)
[32]	$(0.61 + 0.063v_0)v_0^2 \times 10^{-3}$	$6 < v_0 < 22$
[36]	$1.14v_0^2 \times 10^{-3}$	$4 < v_0 < 10$
[36]	$(0.49 + 0.065v_0)v_0^2 \times 10^{-3}$	$10 < v_0 < 26$
[37]	$(0.50 + 0.071v_0)v_0^2 \times 10^{-3}$	$6 < v_0 < 26$
[38]	$[-0.00018v_0^2 + 0.051(v_0 - 8) + 0.027]^2$	$8 < v_0 < 30$

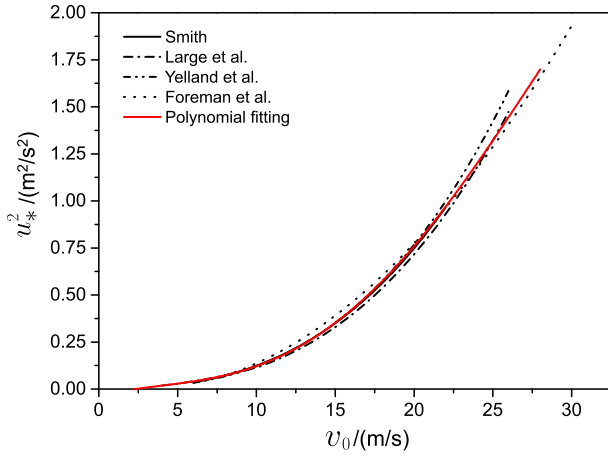


Fig. 1. Relationship between u_*^2 and v_0 . The solid line is the polynomial fitting result of Eq. (11), and the others are from Ref. Smith [32], Large and Pond [36], Yelland and Moat et al. [37] and Foreman and Emeis [38].

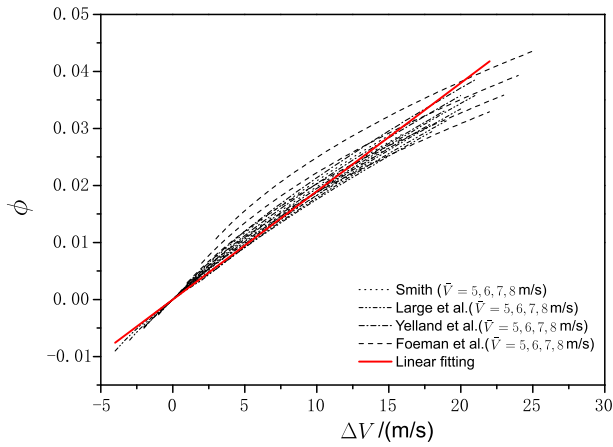


Fig. 2. Plot of function $\phi(\Delta V, \bar{V})$. The solid line is the linear fitting result of Eq. (12) with $\kappa = 0.0019(\text{m/s})^{-1}$, and the other lines are results according to friction velocity from references Smith [32], Large and Pond [36], Yelland and Moat et al. [37] and Foreman and Emeis [38] when \bar{V} equals to 5 m/s, 6 m/s, 7 m/s and 8 m/s.

say 100 m. That is to say the deviation of WPD at a single site due to the simplification of ϕ will be about 3% maximal.

Finally, inserting Eq. (12) into Eq. (8), we have the velocity at height z as Eq. (13), in which $\xi(z, \bar{V})$ is already known using Eqs. (9) and (11).

$$\frac{v(z)}{v_0} = 1 + \xi(z, \bar{V}) + \kappa \ln(z/10) \Delta V. \quad (13)$$

Based on Eqs. (1), (2) and (13), WPD at height z can be written in the form of the central moments of wind speed at reference height as

$$E_z = \frac{1}{2} \rho_0 (1 - \eta) \left[a^3 \bar{V}^3 + c_2 \bar{V} E(\Delta V^2) + c_3 E(\Delta V^3) + c_4 \kappa E(\Delta V^4) + c_5 \kappa^2 E(\Delta V^5) + b^3 \kappa^3 E(\Delta V^6) \right] \quad (14)$$

The non-dimensional coefficients, related to height z and mean wind speed \bar{V} only, are expressed as Eqs. (15)–(20).

$$a = 1 + \xi(z, \bar{V}). \quad (15)$$

$$b = \ln(z/10). \quad (16)$$

$$c_2 = 3a^3 + 9a^2 b \kappa \bar{V} + 3ab^2 \kappa^2 \bar{V}^2. \quad (17)$$

$$c_3 = a^3 + 9a^2 b \kappa \bar{V} + 9ab^2 \kappa^2 \bar{V}^2 + b^3 \kappa^3 \bar{V}^3. \quad (18)$$

$$c_4 = 3a^2 b + 9ab^2 \kappa \bar{V} + 3b^3 \kappa^2 \bar{V}^2. \quad (19)$$

$$c_5 = 3ab^2 + 3b^3 \kappa \bar{V}. \quad (20)$$

$\eta(z)$ the air density adjustment factor can be estimated by Eq. (21) for dry air under the assumption of standard pressure and temperature profiles [39], which is of order of 1% (for example, $\eta(100) \sim O(0.8\%)$).

$$\eta(z) = 1 - \frac{101.29 - 0.011837z + 4.793 \times 10^{-7} z^2}{288.15 - 0.0066z} \frac{1}{\rho_0}. \quad (21)$$

The statistical model Eq. (14) considering sea state effect is consisted of the central moments of wind speed at reference height, which means the vertical structure of WPD can be evaluated handily once wind speed at reference height are recorded. When z equals to 10 m, we have $a = 1$ and $b = 0$ resulting in vanishing of the terms of fourth- to sixth- orders of central moments and $c_3 = 1$, $c_2 = 3$ and $\eta = 0$. Consequently, Eq. (14) degenerates to Eq. (3).

Now, it is necessary to examine the magnitudes of the terms in Eq. (14), so that inconsequential terms can be discarded reasonably. There are six totally non-dimensional coefficients a , b , c_2 , c_3 , c_4 and c_5 in Eq. (14), and they are all monotone increasing functions when \bar{V} or z increases. As for the usual situation: \bar{V} ranges from 5 m/s to 8 m/s and z varies over 50–140 m, a^3 and c_3 are $O(1)$, c_4 and c_5 are $O(10)$, while b^3 and c_2 are intermediate. On the other hand, κ is $O(10^{-3})$ and ΔV is $O(10)$ maximal. Therefore, we can roughly say $b^3 \kappa^3 E(\Delta V^6)$ is about 1% of $c_5 \kappa^2 E(\Delta V^5)$; $c_5 \kappa^2 E(\Delta V^5)$ could not be larger than 1% of $c_4 \kappa E(\Delta V^4)$; and $c_4 \kappa E(\Delta V^4)$ is about 10% of $c_3 E(\Delta V^3)$. That means dropping $c_5 \kappa^2 E(\Delta V^5)$ and $b^3 \kappa^3 E(\Delta V^6)$ only introduces errors less than one thousandth.

Therefore, truncations of WPD under different precisions can be carried out as Eq. (22) and Eq. (23), in which $O(\epsilon_1)$ and $O(\epsilon_2)$ are less than 1% and 10%, respectively. In this work, Eq. (22) is adopted.

$$E_z = \frac{1}{2} \rho_0 (1 - \eta) \left[a^3 \bar{V}^3 + c_2 \bar{V} E(\Delta V^2) + c_3 E(\Delta V^3) + c_4 \kappa E(\Delta V^4) + O(\epsilon_1) \right]. \quad (22)$$

$$E_z = \frac{1}{2} \rho_0 \left[a^3 \bar{V}^3 + c_2 \bar{V} E(\Delta V^2) + c_3 E(\Delta V^3) + O(\epsilon_2) \right]. \quad (23)$$

2.3. Technical potential model

Technical potential here is the wind energy potential with the influential factors such as WPD, geographic constraints, wind turbine size and layout considered. The on land technical wind energy potential is usually calculated by introducing the influences of terrain slope, installed capacity of wind turbines and local WPD class into the theoretical potential [40], which seems unsuitable for the offshore situation. In this work, the offshore technical potential

is examined based on the following model:

$$WP_T = \frac{A_S}{A_T} \cdot E_T \cdot \frac{16}{27} \cdot (1 - C_w). \tag{24}$$

A_S is the geographic area available for developing wind energy with the spatial constraints such as marine reserves, shipping lanes, cables and pipelines excluded. A_T is the averaged area of per wind turbine occupied, which depends on the layout of offshore wind farm, i.e. the space between wind turbines and that between neighboring wind farms. E_T is the kinetic energy of air flowing through the disk swept by the blades, which is estimated by integrating WPD over the disk. The coefficient 16/27 is the well-known Betz limit, and C_w is the loss rate due to wake effect, say 8% [7].

3. Study area and methodology

3.1. Study area

There are five seas along China coast, i.e. Bohai Sea, Yellow Sea, East China Sea and South China Sea from north to south. The area of the five seas with water depth less than 250 m as shown in Fig. 3 is about $9.5 \times 10^5 \text{ km}^2$. It is noteworthy that area around reefs outside the continental shelf was neglected due to their slim contribution to the total technical potential and significant difficulty of development. There are intense shipping traffic and lots of marine reserves located in the study area. The region where water depth larger than 250 m corresponds to the continental slope or deep seas which implies more technical challenges when developing wind farms such as power transmission and suppression of structural motion. As we know, water depth 50–100 m is commonly considered as the transition depth when floating platforms are economical with respect to the bottom fixed turbines [41], and the critical water depth varies for different types of floater and specific sites. Thus, wind resources over regions of water depth 0–50 m (R1),

50–100 m (R2) and 100–250 m (R3) as indicated in Fig. 3 are investigated separately.

3.2. Data source

The wind field data comes from the NASA's Cross-Calibrated, Multi-Platform Ocean Surface Wind Velocity project [23,24]. It combines data from radiometers instrument platforms including SSM/I, SSMIS, AMSR, TMI, Windsat and GMI, and data from scatterometer instrument platforms such as QuikSCAT, Seawinds and ASCAT. Those data are further validated against conventional data including ship and ocean moored buoys observations from the Scientific Division of the National Center for Atmospheric Research (NCAR) and Pacific Marine and Environmental Laboratory (PMEL). Carvalho et al. [42] compared the ocean surface wind data derived from several widely used QuikSCAT products and the CCMP project. They concluded that CCMP wind data has significant improvements in terms of wind direction temporal variability and wind speed mean state, and CCMP wind field data have mitigated some of QuikSCAT's known problems related to QuikSCAT systematic tendency to overestimate the wind speed and land masking effects. To reduce the uncertainties as much as possible, 28 years of wind data from July 1987 to June 2015 with temporal resolution 6 h and spatial resolution $0.25^\circ \times 0.25^\circ$ are adopted in this work.

The bathymetric data is retrieved from the National Centers for Environment Information, which belongs to National Oceanic and Atmospheric Administration (NOAA). In this study, ETOPO1, a 1 arc-minute global relief model of Earth's surface were utilized.

Though offshore region is independent of land slope constraint, spatial constraints such as biodiversity protection area and shipping lanes are still involved. In this work, spatial constraints including shipping lanes, cables and pipelines, bird path and visibility from Ref. [7], exclusive economic zone boundaries database from Marine Regions and marine reserves from Ref. [43] are considered.

3.3. GIS-based assessment

The main steps of the assessment are as follows.

Step i. Based on the assumption of Weibull distributed wind speed, the shape and scaling factors are calculated by the maximum likelihood estimation of the CCMP wind speed series at every grid.

Step ii. WPD at various hub height are estimated according to Eq. (22).

Step iii. Influential factors including WPD, marine reserves, shipping lanes, cables and pipelines, bird path, visibility and exclusive economic zone boundaries are analyzed on the GIS platform.

Step iv. Technical potentials of the study area under different scenarios are obtained according to Eq. (24).

4. Results and discussion

4.1. Influence of sea state effect on WPD

To demonstrate the influence of sea state effect on WPD quantitatively, sixty-seven sites uniformly located in the study area are selected to observe the difference of WPD with sea state effect considered/discarded. The 95% confidence intervals of shape and scaling factors of wind speed series at those sites are presented as shown in Fig. 4. The upper and lower limits of shape factors are in red, and that of scaling factors are in blue. Scatter plot Fig. 4 shows that scaling factors of wind speed series over the study area range

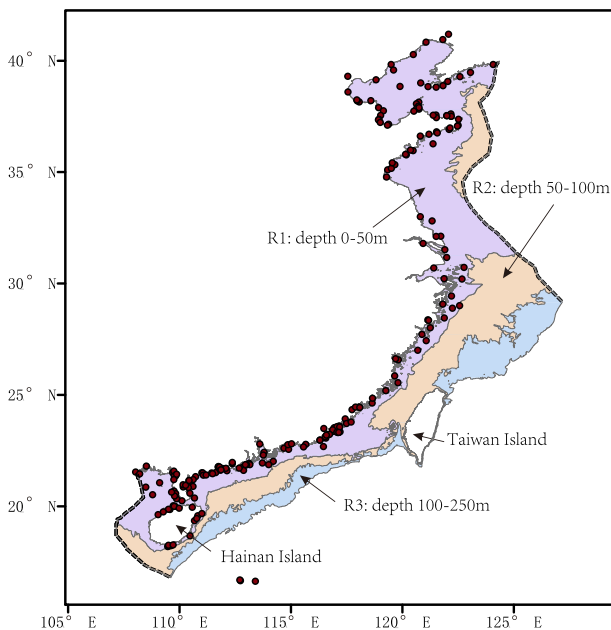


Fig. 3. Overview of the study area. Three regions R1 to R3 marked in purple, incarnadine and blue, respectively, are divided according to the water depth: R1 water depth 0–50 m, R2 water depth 50–100 m and R3 water depth 100–250 m. The dash lines are the exclusive economic zone boundaries. The dots are the marine reserves. (For interpretation of the references to color in this figure legend, the reader is referred to the Web version of this article.)

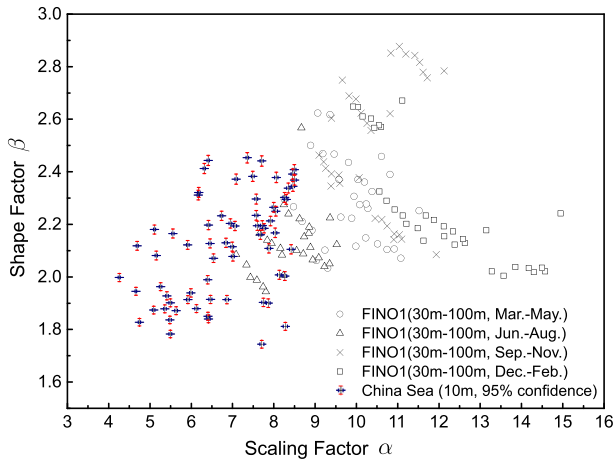


Fig. 4. Shape and scale factors of wind speed series over the study area. The colored crosses with limits are 95% confidence intervals of shape and scaling factors at the selected 67 sites. The black circles, triangle, cross and triangle are shape and scaling factors based on the 10 min averaged wind speed series from FINO1 at eight heights from 30 m to 100 m [44].

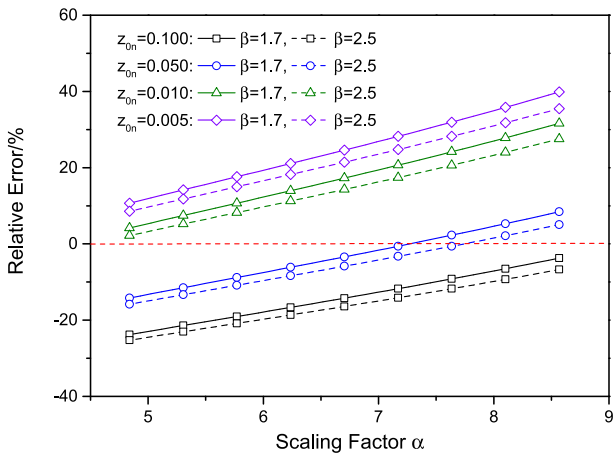


Fig. 5. Relative error of PWD between situations sea state effect discarded and considered. Four constant roughness lengths 0.005 m, 0.01 m, 0.05 m and 0.1 m are chose for the situation of sea state effect discarded.

between 4.5 and 8.5, while shape factors range between 1.7 and 2.5. As a comparison, the shape and scale factors of in-situ measured wind speed series from FINO1 research platform located 45 km north of the island Borkum in the German Bight are presented in Fig. 4 as well. The scaling factors of the study area are smaller than that of FINO1 is due to the different observation height: 10 m for the study area, while 30–100 m for the FINO1.

The relative error (RE) between situations sea state effect discarded and considered is examined for scaling factor $\alpha \in [4.5, 8.5]$ and shape factor $\beta \in [1.7, 2.5]$. As for the sea state effect discarded situation, i.e. a constant sea roughness length is assumed for the study area, four constant roughness lengths are chose: $z_{0n} = 0.005$ m, $z_{0n} = 0.01$ m, $z_{0n} = 0.05$ m and $z_{0n} = 0.1$ m. REs of WPD at height 70 m are presented here as shown in Fig. 5. It shows that REs of WPD at some locations will be as large as 40%, see situation $z_{0n} = 0.005$ m, $\alpha = 8.5$ and $\beta = 1.7$. $z_{0n} = 0.05$ m seems to be the best one out of the four sea roughness lengths considered, however, 16% discrepancy is also observed. According to Fig. 5, using just one constant roughness length, even the optimized one, significant deviation in WPD will be introduced for some locations. That's because it is impossible to capture the sea states at different locations by only one constant roughness length, especially for regional scale wind resource assessment where remarkable disparity of sea state encounters.

4.2. Distribution of wind power density

The geographical distribution of WPD at height 70 m and 110 m are presented in Fig. 6. It demonstrates that the southeast domain including the East China Sea, Taiwan Strait and South China Sea around Northern Guangdong Province are endowed with rich wind resources. Bohai Sea, Yellow Sea and South China Sea around Hainan Island are less windy regions. For 70 m height, WPD ranges from 294 W/m^2 to 1113 W/m^2 (see Fig. 6 (a)). The wind resource in the Taiwan Strait is particularly abundant, where WPD is above 900 W/m^2 . WPD at height 110 m is ranging between 349 W/m^2 and 1270 W/m^2 , which is about 100 W/m^2 larger than those at 70 m roughly.

The vertical variation of spatial-averaged WPD for region R1 to R3 are presented in Fig. 7. Spatial-averaged WPD here refers to the WPD averaged over the concerned area in the geographic coordinate system, which means the spherical effect of the earth is considered. From Fig. 7, WPD grows rapidly with height. As for R1,

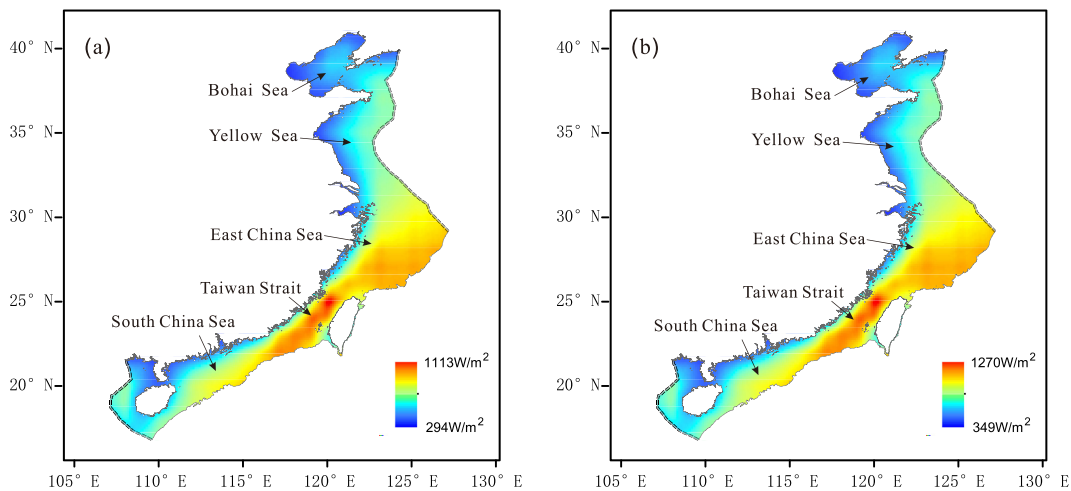


Fig. 6. Geographical distribution of wind power density. (a) and (b) are at height 70 m and 110 m, respectively.

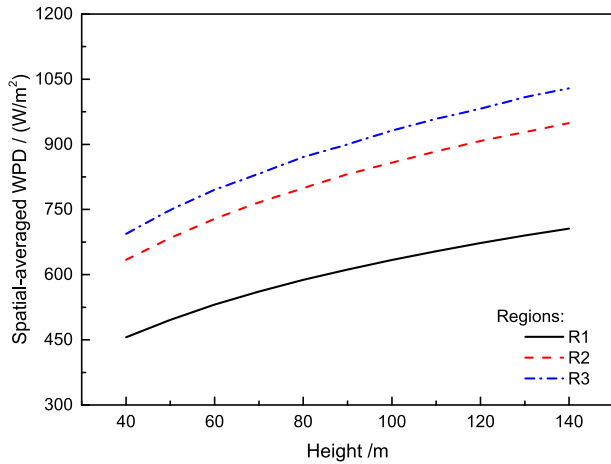


Fig. 7. Vertical variation of the spatial-averaged wind power density. The horizontal axis is the height, and the vertical axis is the spatial-averaged wind power density. The solid, dash and dot-dash lines are for regions R1, R2 and R3, respectively.

WPD ranging from 456 W/m² to 706 W/m² turns out to be much less than that of deeper water depth area, i.e. R2 and R3. WPD of R2 is 634–949 W/m², and difference between R2 and R3 is about 60–80 W/m². That is quite straightforward because wind speed at offshore regions trends to be larger and more steady than the nearshore regions. Literature shows that the critical distance for wind speed transiting from rising to steady stage over the seas of China is about 30–100 km from the coast [5].

4.3. Spatial constrains

There are more than 200 marine reserves which mostly located in the nearshore region as marked by the red dot in Fig. 3. The total area of those marine reserves is about 135,500 km² [43]. The buffers of shipping lanes, cables and pipelines, bird path and visibility considered here are 1 km, 500 m, 3 km and 8 km, respectively. Relied on the GIS platform, geographic area available for developing offshore wind energy are calculated as Table 2. It demonstrates that area suitable for developing offshore wind energy are 1.99 × 10⁵ km², 3.25 × 10⁵ km² and 1.91 × 10⁵ km² for regions R1 to R3, respectively. We may observe that the spatial constraints have significant impact on the nearshore regions, i.e. only 48.1% of area of R1 is free of spatial constraints. As for the regions of deeper water depth, R2 and R3, the influences of spatial constraints are obviously minor only about 4.4% and 1.8%, respectively.

4.4. Technical potential

Hub height *H* and rotor radius *R* (or rotor diameter *D*) affect the technical potential via the kinetic energy of air through the disk area *E_T* and the average occupancy area of per wind turbine *A_T*. Rotor radius and hub height depend on the specific type of wind

Table 2 Available area for developing offshore wind energy considering spatial constraints (10⁵ km²). Other spatial constraints here includes shipping lanes, cables and pipelines, bird path and visibility.

Regions	Total area	Marine reserves	Other constraints	A _S
R1	414.7	111.2	104.2	199.3
R2	340.4	0	15.1	325.3
R3	194.7	0	3.5	191.2

Table 3 Scenarios of wind farm layout.

Scenario	Turbine spacing	Row	Column	Buffer of neighboring farms
S1	8 <i>D</i> × 8 <i>D</i>	8	15	20 km
S2	10 <i>D</i> × 5 <i>D</i>	8	15	20 km
S3	10 <i>D</i> × 10 <i>D</i>	8	15	20 km

turbine, for example, that of 5 MW wind turbine are about 63 m and 90 m [25], while that for a 10 MW wind turbine are 75 m and 120 m [26]. In this study, the rotor radius 30 m ≤ *R* ≤ 110 m and hub heights *R* + 10 m ≤ *H* ≤ *R* + 30 m are analyzed. The layout of offshore wind farm also has significant impact on the technical potential, which is usually related to the rotor diameter *D*. Mentis et al. [45] used the layout that turbines are spaced 10*D* apart in the prevailing direction and 5*D* apart in crosswind direction, which is also the layout of Denmark’s Tuno Knob offshore wind farm. Two wind farm layouts 10*D* × 10*D* and 10*D* × 5*D* are examined by Li [46]. Hong et al. [7] used the layout that each offshore wind farm is consisted of 8 turbines a row and 15 turbines a column, the distance among wind turbines are 8*D*, and a 20 km buffer region is arranged between neighboring wind farms. Accordingly, three wind farm layouts, S1–S3, as given in Table 3 are produced to examine their influence on technical potential.

Technical potential of the study area for layouts S1–S3 are presented as shown in Fig. 8. It shows that technical potential increases with rotor radius increases. Taking layout scenario S1 as an example: for rotor radius 60 m, the technical potentials for R1 to R3 are 139 GW, 308 GW and 166 GW, respectively; while that for rotor radius 90 m are 288 GW, 635 GW and 341 GW, respectively. That is to say technical potential is quite sensitive to the size of wind turbine. Roughly speaking, the growth rates of technical potential with rotor radius are: 4.6 GW/m for R1 (see Fig. 8(a)), 9.3 GW/m for R2 (see Fig. 8(b)) and 5.4 GW/m for R3 (see Fig. 8(c)). Hub height has minor influence on the technical potential as indicated by the red error bar.

Comparing Fig. 8(a) with (b) and (c), we can see that the technical potential of R1 is only about 23% of that of the study area. Thus, developing economical wind turbine capable of harvesting wind energy at water depth above 50 m, e.g. floating wind turbine, seems worthy of consideration. As we know, most of the floating wind turbine projects are in the conceptual design phase at present except for a very few projects such as Hywind, WindFloat, Fukushima [41]. Fig. 8(b) and (c) demonstrate that technical potential of R3 is much smaller than that of R2, though WPD over R3 is larger than that of R2. That’s because the geographic area available for developing wind energy of R3 is only 59% of R2, see Table 2.

The technical potential for layouts S1, S2 and S3 are provided by different linetype as shown in Fig. 8 as well. It demonstrates that technical potential is significantly influenced by the wind farm layout. As for the three layouts considered in this study (see Table 3), technical potential of layout S1 and S2 have negligible difference, while that of layout S3 is about 4.8%–13.9% less. Besides the spacing between wind turbines, buffer between neighboring wind farms may also considerably affect the technical potential. Actually, the area of the buffer regions is far more larger than that occupied by the wind farm itself. That opens the possibility to eliminate the influence of spatial constraints to a certain degree by careful arrangement of spatial constraints in the buffer regions. Under this circumstances, the technical potential of R1 can be doubled at most. Taking layout S1 as an example, the total technical potential could probably be enhanced up to 752 GW and 1522 GW maximal for rotor radius 60 m and 90 m, respectively.

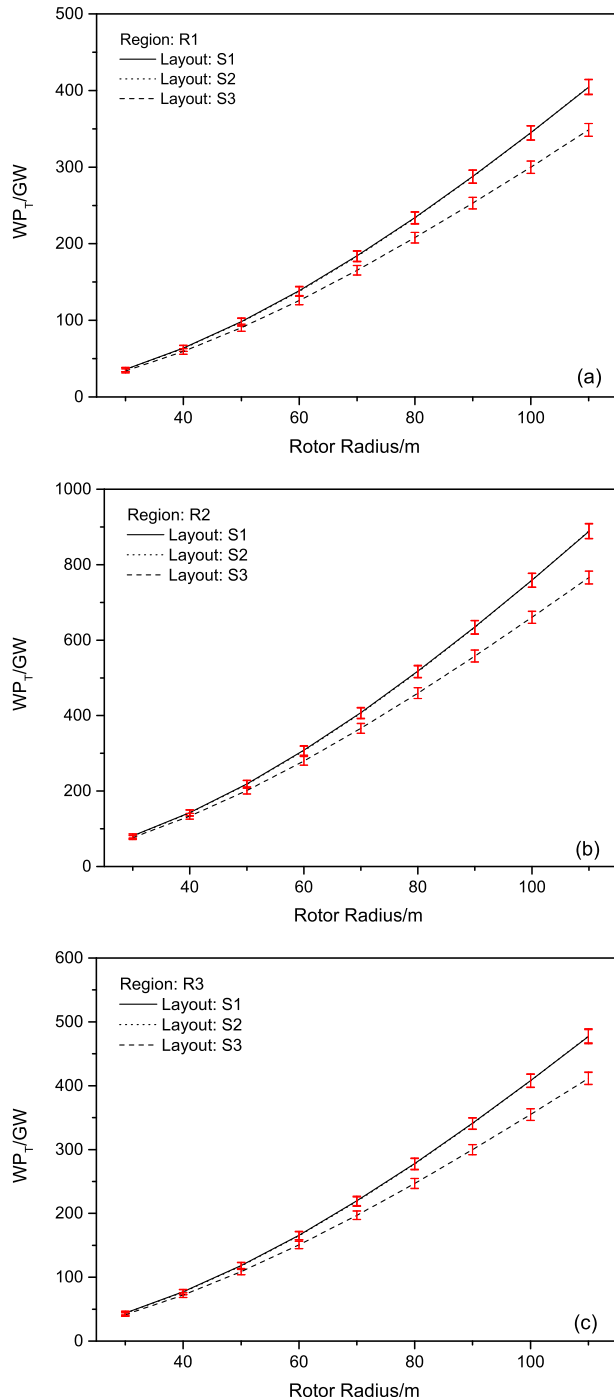


Fig. 8. Technical potential for different rotor radii, hub heights and layouts. The solid, short dash and dash lines are technical potential for layouts S1, S2 and S3, respectively (see Table 3). The red error bar is introduced by the variation of hub heights. (a), (b) and (c) are for regions R1, R2 and R3, respectively. Since technical potentials for layout S1 and S2 have minor difference, the short dash and solid lines are almost overlapped.

5. Conclusions

Technical potential of offshore wind resource over the sea area shallower than 250 m along China coast is investigated using 28 years CCMP wind field data. To avoid erroneous estimation of wind power density due to sea state effect, a statistical technical wind energy potential model filling the gap between the present understanding of marine boundary layer and the requirement of

regional offshore wind resource assessment is proposed firstly. Influential factors related to developing offshore wind energy such as wind power density, water depth, wind farm layout and various spatial constraints are examined on the GIS platform. Technical potential for different scenarios are presented as shown in Fig. 8.

The main results are:

- Neglecting sea state effect by assuming a constant roughness length for the study area, even the optimized one, can implement significant deviation in the wind power density during regional scale offshore wind resource assessment.
- The Southeast domain including the East China Sea, Taiwan Strait and South China Sea around Northern Guangdong Province are endowed with rich wind resources. Bohai Sea, Yellow Sea and South China Sea around Hainan Island are less windy regions. Wind resource in the Taiwan Strait is particularly abundant, where wind power density at 70 m height can be above 900 W/m^2 .
- Technical potential is quite sensitive to the size of wind turbine. Taking layout scenario S1 (see Table 3) as an example: for rotor radius 60 m, the technical potential for regions water depth 0–50 m, 50–100 m and 100–250 m are 139 GW, 308 GW and 166 GW, respectively; while that for rotor radius 90 m are 288 GW, 635 GW and 341 GW, respectively. Roughly speaking, the growth rates of technical potential with rotor radius for the aforementioned three regions are: 4.6 GW/m, 9.3 GW/m and 5.4 GW/m, respectively.
- Only 48.1% of area for water depth 0–50 m is free of spatial constraints. Optimizing the macro-siting of wind farms by arranging the spatial constraints in the buffer region between neighboring wind farms may eliminate the influence of spatial constraints markedly.

Those results are expected to provide valuable information for the future offshore wind energy planning and the development of new wind turbines.

Acknowledgement

The authors greatly appreciate Prof. He Dexin for his helpful discussions and suggestions on the present work. This work is supported by China Postdoctoral Science Foundation (2017M620597) and National Natural Science Foundation of China (1172339 and 11232012).

References

- [1] Global Wind Energy Council, Global Wind Report: Annual Market Update, Tech. rep., Global Wind Energy Council Document (2011, 2012, 2013, 2014, 2015, 2016, 2017).
- [2] G. Corbetta, A. Ho, I. Pineda, Wind Energy Scenarios for 2030, Tech. rep., European Wind Energy Association Document, 2016.
- [3] A. Smith, T. Stehly, W. Musial, 2014–2015 Offshore Wind Technologies Market Report, Tech. rep., National Renewable Energy Laboratory Document, 2015.
- [4] Chinese National Energy Administration, The Electric Power Development Planning in 13th Five-year (2016–2020), Tech. rep., Chinese National Energy Administration Document, 2016.
- [5] Z.N. xiao, R. Zhu, L.L. Song, Z.X. Zhi, et al., China's Wind Power Resource Evaluation Report 2009, China Meteorological Press, 2009.
- [6] H. Qin, M. Liu, Y. Wang, J. Zhao, X. Zeng, R. Reinvang, R. Enslow, H. Beaumont, China: an Emerging Offshore Wind Development Hotspot—with a New Assessment of Chinas Offshore Wind Potential, Tech. rep., Chinese Wind Energy Association, 2010.
- [7] L. Hong, B. Möller, Offshore wind energy potential in China: under technical, spatial and economic constraints, Energy 36 (7) (2011) 4482–4491.
- [8] D. Li, B. Geyer, P. Bisling, A model-based climatology analysis of wind power resources at 100-m height over the bohai sea and the yellow sea, Appl. Energy 179 (2016) 575–589.
- [9] X. Lu, M.B. McElroy, C.P. Nielsen, X. Chen, J. Huang, Optimal integration of offshore wind power for a steadier, environmentally friendlier, supply of

- electricity in China, *Energy Pol.* 62 (2013) 131–138.
- [10] R. Chang, R. Zhu, M. Badger, C.B. Hasager, R. Zhou, D. Ye, X. Zhang, Applicability of synthetic aperture radar wind retrievals on offshore wind resources assessment in hangzhou bay, China, *Energies* 7 (5) (2014) 3339–3354.
- [11] R. Chang, R. Zhu, M. Badger, C.B. Hasager, X. Xing, Y. Jiang, Offshore wind resources assessment from multiple satellite data and wrf modeling over South China Sea, *Rem. Sens.* 7 (1) (2015) 467–487.
- [12] B. Jiang, X.L. Yang, S. Zhang, J.Y. Xing, Z.Z. Ma, Ocean wind energy resource assessment on China's offshore by using mm5 model, *Wind Energy (in Chinese)* 03 (2013) 150–163.
- [13] D. Jiang, D.F. Zhuang, Y.H. Huang, J.H. Wang, J.Y. Fu, Evaluating the spatio-temporal variation of China's offshore wind resources based on remotely sensed wind field data, *Renew. Sustain. Energy Rev.* 24 (2013) 142–148.
- [14] A. Ulazia, J. Saenz, G. Ibarra-Berastegui, Sensitivity to the use of 3dvar data assimilation in a mesoscale model for estimating offshore wind energy potential. a case study of the iberian northern coastline, *Appl. Energy* 180 (2016) 617–627.
- [15] C. Mattar, D. Borvarán, Offshore wind power simulation by using wrf in the central coast of Chile, *Renew. Energy* 94 (2016) 22–31.
- [16] G. Amirinia, B. Kamranzad, S. Mafi, Wind and wave energy potential in southern caspian sea using uncertainty analysis, *Energy* 120 (2017) 332–345.
- [17] M.J. Dvorak, C.L. Archer, M.Z. Jacobson, California offshore wind energy potential, *Renew. Energy* 35 (6) (2010) 1244–1254.
- [18] H.-F. Fang, Wind energy potential assessment for the offshore areas of taiwan west coast and penghu archipelago, *Renew. Energy* 67 (2014) 237–241.
- [19] I. Balog, P.M. Ruti, I. Tobin, V. Armenio, R. Vautard, A numerical approach for planning offshore wind farms from regional to local scales over the mediterranean, *Renew. Energy* 85 (2016) 395–405.
- [20] S.B. Capps, C.S. Zender, Estimated global ocean wind power potential from quikscat observations, accounting for turbine characteristics and siting, *J. Geophys. Res.: Atmos.* 115 (2010), D09101.
- [21] C.B. Hasager, M. Badger, A. Peña, X.G. Larsén, F. Bingöl, Sar-based wind resource statistics in the baltic sea, *Rem. Sens.* 3 (1) (2011) 117–144.
- [22] S. Gadad, P.C. Deka, Offshore wind power resource assessment using Oceansat-2 scatterometer data at a regional scale, *Appl. Energy* 176 (2016) 157–170.
- [23] R. Atlas, R.N. Hoffman, J. Ardizzone, S.M. Leidner, J.C. Jusem, D.K. Smith, D. Gombos, A cross-calibrated, multiplatform ocean surface wind velocity product for meteorological and oceanographic applications, *Bull. Am. Meteorol. Soc.* 92 (2) (2011) 157–174.
- [24] F. Wentz, J. Scott, R. Hoffman, M. Leidner, R. Atlas, J. Ardizzone, Remote Sensing Systems Cross-calibrated Multi-platform (Ccmp) 6-hourly Ocean Vector Wind Analysis Product on 0.25 Deg Grid, version 2.0, Remote Sensing Systems, Santa Rosa, CA. Available online at: www.remss.com/measurements/ccmp.
- [25] S. Krohn, P.-E. Morthorst, S. Awerbuch, *The Economics of Wind Energy*, European Wind Energy Association, 2009.
- [26] R. Swart, C. Coppens, H. Gordijn, M. Piek, P. Ruysenaars, J. Schrande, P. de Smet, M. Hoogwijk, M. Papalexandrou, E. de Visser, et al., Europe's Onshore and Offshore Wind Energy Potential: an Assessment of Environmental and Economic Constraints, Tech. rep., European Environment Agency, 2009.
- [27] Z.R. Shu, Q.S. Li, Y.C. He, P.W. Chan, Observations of offshore wind characteristics by Doppler-lidar for wind energy applications, *Appl. Energy* 169 (2016) 150–163.
- [28] X. Gao, H. Yang, L. Lu, Study on offshore wind power potential and wind farm optimization in Hong Kong, *Appl. Energy* 130 (2014) 519–531.
- [29] S. Emeis, *Wind Energy Meteorology: Atmospheric Physics for Wind Power Generation*, Springer Science & Business Media, 2012.
- [30] G. Amirinia, S. Mafi, B. Kamranzad, Offshore wind resource assessment of Persian gulf using uncertainty analysis and gis, *Renew. Energy* 113 (2017) 915–929.
- [31] A. Sathe, *Atmospheric Stability and Wind Profile Climatology over the North Sea: Case Study at Egmond Aan Zee, Torque 2010: the Science of Making Torque from Wind*, Heraklion, Crete, Greece, 2010, pp. 395–405.
- [32] S.D. Smith, Wind stress and heat flux over the ocean in gale force winds, *J. Phys. Oceanogr.* 10 (5) (1980) 709–726.
- [33] P.P. Sullivan, J.C. McWilliams, Dynamics of winds and currents coupled to surface waves, *Annu. Rev. Fluid Mech.* 42 (2010) 19–42.
- [34] J. Li, Z. Zhang, Two-parameter-dependent drag coefficient over sea surface by turbulent modeling, *Commun. Nonlinear Sci. Numer. Simulat.* 4 (1) (1999) 8–11.
- [35] N. Maat, C. Kraan, W. Oost, The roughness of wind waves, *Boundary-Layer Meteorol.* 54 (1–2) (1991) 89–103.
- [36] W. Large, S. Pond, Open ocean momentum flux measurements in moderate to strong winds, *J. Phys. Oceanogr.* 11 (3) (1981) 324–336.
- [37] M. Yelland, B. Moat, P. Taylor, R. Pascal, J. Hutchings, V. Cornell, Wind stress measurements from the open ocean corrected for airflow distortion by the ship, *J. Phys. Oceanogr.* 28 (7) (1998) 1511–1526.
- [38] R.J. Foreman, S. Emeis, Revisiting the definition of the drag coefficient in the marine atmospheric boundary layer, *J. Phys. Oceanogr.* 40 (10) (2010) 2325–2332.
- [39] J. Manwell, J. McGowan, A. Rogers, *Wind Energy Explained: theory, Design and Application*, John Wiley & Sons, Ltd, 2002.
- [40] D. Kline, D. Heimiller, S. Cowlin, *A GIS Method for Developing Wind Supply Curves*, National Renewable Energy Laboratory, 2008.
- [41] M. Karimirad, *Offshore Energy Structures—for Wind Power, Wave Energy and Hybrid Marine Platforms*, Springer, 2014.
- [42] D. Carvalho, A. Rocha, M. Gómez-Gesteira, I. Alvarez, C.S. Santos, Comparison between ccmp, quikscat and buoy winds along the iberian peninsula coast, *Rem. Sens. Environ.* 137 (2013) 173–183.
- [43] J.L. Zeng, *Marine reserves of China*, China Ocean Press, 2014.
- [44] M. Bilstein, S. Emeis, The annual variation of vertical profiles of weibull parameters and their applicability for wind energy potential estimation, *DEWI Mag.* 36 (2010) 44–48.
- [45] D. Mentis, S. Hermann, M. Howells, M. Welsch, S.H. Siyal, Assessing the technical wind energy potential in africa a gis-based approach, *Renew. Energy* 83 (2015) 110–125.
- [46] G. Li, Feasibility of large scale offshore wind power for Hong Kong—a preliminary study, *Renew. Energy* 21 (3) (2000) 387–402.